J Comput Neurosci
DOI 10.1007/s10827-008-0097-3

Parametric and non-parametric modeling of short-term synaptic plasticity. Part I: computational study

Dong Song · Vasilis Z. Marmarelis · Theodore W. Berger

Received: 21 November 2007 / Revised: 8 April 2008 / Accepted: 1 May 2008

Abstract Parametric and non-parametric modeling methods are combined to study the short-term plasticity (STP) of synapses in the central nervous system (CNS). The nonlinear dynamics of STP are modeled by means: (1) previously proposed parametric models based on mechanistic hypotheses and/or specific dynamical processes, and (2) non-parametric models (in the form of Volterra kernels) that transforms the presynaptic signals into postsynaptic signals. In order to synergistically use the two approaches, we estimate the Volterra kernels of the parametric models of STP for four types of synapses using synthetic broadband input–output data. Results show that the non-parametric models accurately and efficiently replicate the input–output transformations of the parametric models. Volterra kernels provide a general and quantitative representation of the STP.

Keywords Facilitation · Depression · Nonlinear modeling · Poisson random train · Volterra kernels

Action Editor: David Golomb

D. Song (✉) · V. Z. Marmarelis · T. W. Berger
Department of Biomedical Engineering,
University of Southern California,
403 Hedco Neuroscience Building,
Los Angeles, CA 90089, USA
e-mail: dsong@usc.edu

T. W. Berger
Program in Neuroscience, University of Southern California,
Los Angeles, USA

D. Song · V. Z. Marmarelis · T. W. Berger
Center for Neural Engineering, University of Southern California,
Los Angeles, USA

1 Introduction

Short-term synaptic plasticity (STP) is the use-dependent alteration in the strength of synaptic transmission over a time scale of milliseconds to seconds, whereby the magnitudes of postsynaptic responses are dynamically affected by the pattern of recent input impulses (Zucker and Regehr 2002). This is illustrated in Fig. 1, where a train of presynaptic action potentials (inputs) is shown to elicit postsynaptic responses (outputs) with varying amplitudes depending on the temporal pattern of previous presynaptic activity. This phenomenon may also be viewed as a dynamic nonlinearity (Sclabassi et al. 1988; Berger et al. 1994). STP is considered a critical component of synaptic transmission and information processing in the brain (Orban et al. 1985; Reid et al. 1991; Abbott et al. 1997; Lisman 1997; Zador and Dobrunz 1997).

The study on STP dates back to the 1940s (Eccles et al. 1941; Feng 1941). Many underlying mechanisms of STP have been inferred from numerous studies involving various experimental techniques and preparations (Katz and Miledi 1968; Creager et al. 1980; Debanne et al. 1996; Dobrunz and Stevens 1997; Dittman and Regehr 1998; Hanse and Gustafsson 2001). These mechanisms are generally classified into two major categories: facilitation (when the presence of previous presynaptic events causes increased postsynaptic response at present) and depression (when the opposite effect occurs). The most widely accepted biological mechanisms for such STP effects are the residual calcium hypothesis of facilitation and the depletion model of depression (Liley and North 1953; Katz and Miledi 1968; Betz 1970). According to these hypotheses, facilitation is caused by the accumulation of residual calcium in the presynaptic bouton, while depression is due to the depletion of the neurotransmitter vesicle pool.

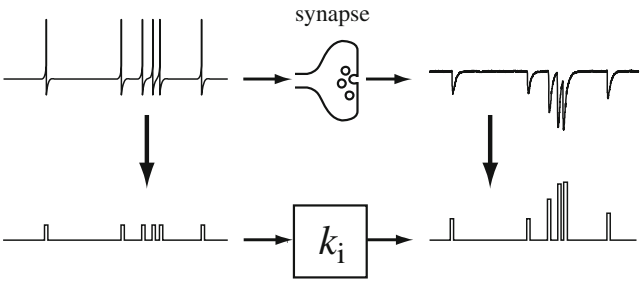

Fig. 1 Illustration of the input–output data representation for the synapse model

Additionally, the recovery of the depleted vesicle pool has been shown to be dependent on the residual calcium concentration (Dittman and Regehr 1998; Wang and Kaczmarek 1998; Hosoi et al. 2007). Depletion-independent mechanisms of depression were also reported (Hsu et al. 1996; Dobrunz et al. 1997; Kraushaar and Jonas 2000; Waldeck et al. 2000; Gover et al. 2002; Kirischuk et al. 2002; Pedroarena and Schwarz 2003; Fuhrmann et al. 2004). Furthermore, postsynaptic mechanisms (e.g., the desensitization of AMPA receptors) are potential contributors to synaptic depression (Trussell and Fischbach 1989; Trussell et al. 1993; Jones and Westbrook 1996).

Many STP models have been developed with distinct scientific aims (Mallart and Martin 1967; Friesen 1975; Magleby and Zengel 1975; Krausz and Friesen 1977; Zengel and Magleby 1982; Yamada and Zucker 1992; Sen et al. 1997; Tsodyks and Markram 1997; Varela et al. 1997; Tsodyks et al. 1998; Hunter and Milton 2001). In one approach, the model is built to explain the physiological mechanisms underlying synaptic transmission. One excellent example of such model was proposed by Dittman et al. (2000). In their model, the STP dynamics is described by the interplay between facilitation, depression and residual calcium at the presynaptic terminal. This type of model can be termed "parametric model" due to the fact that it is expressed with very specific model structures/functions inspired by physiological mechanisms, and a number of adjustable parameters that can be related to certain biological processes. It has a predictive power in uncovering the nature of the underlying physiological processes/mechanisms. For example, by altering the values of its key model parameters, e.g., initial release probability of synapse, one can replicate several distinct forms of STP dynamical characteristics in a physiologically interpretable manner. In terms of reproducing the STP dynamics, such models are often qualitative due to the aim it is developed for.

The other class of STP models were developed to quantitatively identify/replicate the nonlinear dynamical input–output characteristics of STP (Krausz and Friesen 1977; Zengel and Magleby 1982; Sen et al. 1997; Varela et al. 1997). This can be done in a parametrical fashion: the model structure can be determined based on the principle physiological mechanisms, e.g., facilitation and depletion for STP. The values of the unknown parameters can then be estimated from experimental data so that the resulted model replicated the nonlinear dynamical input–output transformation with minimum error. However, for this specific modeling aim, the parametric modeling approach has the inherent limitations associated with their fixed model structure that is determined *a priori* based on the partial knowledge and assumptions to the modeled system, and thus is subject to potential biases. For example, there almost certainly exist unknown mechanisms/processes that are not described by the parametric model. A secondary source of errors may be the accuracy of the required parameter estimation under realistic input characteristics if the parameter estimation is performed on the basis of input–output data obtained with highly specific experimental protocols that contains built-in biases. The latter provide only limited information about the functional characteristics of the system and may bias the estimated parameter values.

An alternative approach is the use of "non-parametric" models that are obtained directly from input–output data collected under broader experimental conditions (e.g. random stimuli that probe the system function with a broader repertoire of inputs) within the framework of a general model form (the functional Volterra series). In the non-parametric modeling approach, no specific assumptions are made *a priori* about the model structure, since the model takes a general form that is applicable to almost all causal systems (Krausz and Friesen 1977; Marmarelis and Marmarelis 1978; Bishop 1995; Marmarelis 2004). Instead of searching for the proper parameter values within a postulated model structure, the non-parametric approach searches for the optimal *functions* (Volterra kernels) contained within the general model that represents the input–output relationship of the system. The nonlinear dynamics underlying synaptic STP can be represented quantitatively by the kernels of the Volterra model that has predictive capability for broadband data. The key point is that the non-parametric model utilizes a general model form (Volterra kernels), thus avoids potential errors in the postulation of the model structure—as required in the parametric modeling approach. The unknown quantities in the non-parametric Volterra model are the *kernels* that are estimated from input–output data collected under broadband conditions (e.g. random inputs). Thus, the non-parametric model, being inductive on the basis of broadband data, has the potential to captures the *complete* input–output nonlinear dynamical characteristics of STP, as determined by all relevant biological processes and underlying mechanisms active under the broadband conditions (Marmarelis and Marmarelis 1978; Berger et al. 1988a; Marmarelis 2004).

As stated above, since parametric and non-parametric models are developed for distinct aims and lay emphasis on different aspects of the modeled system, they are complementary in nature. The main aim of these two papers is to combine both parametric and non-parametric modeling methods in a synergistic manner to study the STP. In this paper (part I), we introduce a recently developed variant of Volterra modeling that employs Laguerre expansions and allows efficient high-order model representation and accurate kernel estimation with short input–output datasets (Marmarelis 1993). This method was applied to overcome the major difficulty of the non-parametric model—its representational complexity caused by the possible high-order kernels required for completeness. We estimated non-parametric models of four different types of central synapses using synthetic broadband input–output data simulated with published parametric models of STP (Varela et al. 1997; Dittman et al. 2000). Results show that the non-parametric models accurately capture the input–output relations defined by the respective parametric models of STP for a broad repertoire of input patterns similar to those encountered under physiological conditions. The effects of specific parameters of the parametric models on the system input–output transformation are reflected directly on specific features of the estimated kernels.

More importantly, since the non-parametric (Volterra) model constitutes a canonical and complete representation of the system (nonlinear) dynamics and it is not restricted by any prior assumptions, it forms a model-free, nearly direct representation of the input–output data themselves. The non-parametric model estimated from experimental data can be used as the "ground truth" to evaluate parametric models of the system in terms of their input–output transformational properties. Furthermore, the non-parametric model may suggest specific modifications in the structure of the respective parametric model. This combined utility of parametric and non-parametric modeling methods is presented in the companion paper (part II).

2 Materials and methods

The input–output data used in this study result from the simulation of the parametric models described below. The data are analyzed according to the Volterra modeling methodology and its recent refinements (i.e. Laguerre expansions of the Volterra kernels) that are also described below.

2.1 Representation of the input–output data

In actual experiments, the input signals at the synapses are trains of action potentials propagating along the axon and delivered at the presynaptic sites of the axon terminals. Since all action potentials have very short duration (1–2ms) and almost identical shapes, they are simplified for purposes of processing and analysis as sequences of discrete impulses (Kronecker delta functions) with inter-impulse intervals encoding the input information. The output signals are the quantities of neurotransmitter released from the vesicles of the presynaptic bouton in response to each action potential arriving at the presynaptic site of the axon terminal. Experimentally, the strengths of neurotransmitter release events are quantified as amplitudes of the excitatory postsynaptic currents (EPSCs). The EPSC trains are simplified as sequences of discrete impulses with varying amplitudes through deconvolution with an EPSC template (see companion paper for more details). The latencies of the EPSCs are short and approximately constant (typically a fraction of 1ms) and thus can be ignored. The EPSCs are recorded under voltage-clamp conditions and after pharmacological manipulations so that the contribution of postsynaptic processes which may introduce nonlinearities (e.g., NMDA current and nonlinear dendritic integration) are diminished. However, strong nonlinearities due to the processes of presynaptic facilitation and depression are maintained, as evidenced by the presented results (see next section) of nonlinear modeling of the input–output data. The computational form of sequences of discrete impulses for the input (fixed amplitude) and output (variable amplitude) is used for the generation of the simulation data. An illustration of the input–output data representation is shown in Fig. 1.

2.2 Parametric models of the four central synapses

The parametric models of four types of CNS synapses having different characteristics of STP are included in this study: (1) the hippocampal CA3-to-CA1 Schaffer collateral synapse (SC); (2) the cerebellar granule cell parallel fiber-to-Purkinje cell synapse (PF); (3) the inferior olive climbing fiber-to-Purkinje cell synapse (CF); and (4) the excitatory synapse in layer 2/3 of the visual cortex (VC).

The EPSC amplitudes for the first three synapses are calculated through simulation of the *FD* model based on the residual calcium hypothesis (Dittman et al. 2000) under conditions of random stimulation (Poisson random impulse trains) using the following equations with different sets of model parameters for each synapse. The EPSCs of the VC synapse are simulated using the FD_1D_2 model (Varela et al. 1997).

The output EPSC of the *FD* model is described by the following equation:

$$\mathrm{EPSC}(t) = \alpha \times N_{\mathrm{T}} \times F(t) \times D(t). \quad (1)$$

where α is the average mEPSC size, N_{T} is the total number of release sites, $F(t)$ is the dynamical facilitation factor and

$D(t)$ is the dynamical depression factor. The product FD is equal to the release probability of the synapses. The dynamical facilitation and depression factors are described by the equations:

$$F(t) = F_1 + \frac{1 - F_1}{1 + K_F / CaX_F(t)}, \tag{2}$$

$$\frac{\partial D}{\partial t} = (1 - D(t)) \times k_{\mathrm{re}\,cov}(CaX_D) - D(t_0) \times F(t_0) \times \delta(t - t_0), \tag{3}$$

$$k_{\mathrm{recov}}(\mathrm{Ca}\,X_{\mathrm{D}}) = \frac{k_{\max} - k_0}{1 + K_D / \mathrm{Ca}\,X_D(t)} + k_0, \tag{4}$$

where F_1 is the initial probability of release, $\mathrm{Ca}X_{\mathrm{F}}$ and $\mathrm{Ca}X_{\mathrm{D}}$ are two putative calcium-bound molecules responsible for facilitation and depression, respectively, K_{F} is the affinity of $\mathrm{Ca}X_{\mathrm{F}}$ for the respective release site, K_{D} is the affinity of $\mathrm{Ca}X_{\mathrm{D}}$ for the respective release site, and k_{recov} is the residual calcium-dependent recovery of depletion that is bounded by the baseline rate of recovery from refractory state k_0 and the maximum rate of recovery from refractory state $k_{\max}$. Eq. (2) defines an instantaneous, nonlinear sigmoidal relation between $\mathrm{Ca}X_{\mathrm{F}}$ and F that bounds F between F_1 and 1. Eq. (3) describes the dynamic changes of the depression factor caused by depletion of the release sites. When a release happens at t_0, the depression factor D decreases by the amount of release $D(t_0)F(t_0)$ since these release sites fall into the refractory period. The rate of recovery k_{recov} is determined by the dynamical concentration of $\mathrm{Ca}X_D$ according to Eq. (4) that models the residual calcium-dependent recovery of depletion and mathematically bounds k_{recov} between k_0 and $k_{\max}$.

The dynamical concentrations of $\mathrm{Ca}X_F$ and $\mathrm{Ca}X_D$ are described by the following two first-order differential equations:

$$\frac{\partial\,\mathrm{Ca}\,X_{\mathrm{F}}}{\partial t} = -\mathrm{Ca}\,X_{\mathrm{F}}(t)/\tau_{\mathrm{F}} + \Delta_{\mathrm{F}} \times \delta(t - t_0), \tag{5}$$

$$\frac{\partial\,\mathrm{Ca}\,X_{\mathrm{D}}}{\partial t} = -\mathrm{Ca}\,X_{\mathrm{D}}(t)/\tau_{\mathrm{D}} + \Delta_{\mathrm{D}} \times \delta(t - t_0). \tag{6}$$

In Eqs. (5) and (6), the concentrations $\mathrm{Ca}X_{\mathrm{F}}$ and $\mathrm{Ca}X_{\mathrm{D}}$ are modeled as two linear processes that decay exponentially with time constants τ_{F} and τ_{D}, after an impulsive change Δ_{F} and/or Δ_{D} of the facilitation and/or depression factor, respectively—triggered by an action potential arriving at the presynaptic site at time t_0.

Since the modeled STP nonlinear dynamics depend only on dimensionless parameters, without loss of generality, the two scalars, α and N_{T}, in Eq. (1) and the impulsive changes Δ_{F} and Δ_{D} are set equal to 1. Note that in Table 1, the equivalent parameter for maximum paired-pulse facilitation ratio ρ is listed instead of K_{F} (Dittman et al. 2000). Their relation is given by:

$$K_F/\Delta_F = \frac{1 - F_1}{(F_1/(1 - F_1)) \times \rho - F_1} - 1, \tag{7}$$

where ρ explicitly models the paired-pulse facilitation ratio for the minimum inter-impulse interval and is the key parameter of facilitation.

In the case of the fourth synapse, the excitatory synapse in layer 2/3 of the visual cortex (VC), the EPSCs are calculated through simulation of the FD_1D_2 model under conditions of random stimulation (Poisson random impulse trains) using the following equations (Varela et al. 1997):

$$A = A_0 \times F \times D_1 \times D_2, \tag{8}$$

Table 1 Parameter values used for the simulation of the models of the four types of synapses

		SC	PF	CF	VC	
Parametric model	*FD*-residual calcium model				FD_1D_2 model	
	P	2.2	3.1	–	A_0	1
	F_1	0.24	0.05	0.35	τ_{F}	94 ms
	τ_{F}	100 ms	100 ms	–	τ_{D1}	380 ms
	τ_{D}	50 ms	50 ms	50 ms	τ_{D2}	9200 ms
	k_0	2 s^{-1}	2 s^{-1}	0.7 s^{-1}	f	0.917
	$k_{\max}$	30 s^{-1}	30 s^{-1}	20 s^{-1}	d_1	0.416
	K_{D}	2	2	2	d_2	0.975
Non-parametric model	PV kernel models					
	L	4	4	4	10	
	M	2000 ms	2000 ms	2000 ms	20 s	
	α	0.984	0.984	0.990	0.998	
	N	400	400	400	2000	

$$F \rightarrow F + f, \tag{9}$$

$$D \rightarrow D \times d, \tag{10}$$

$$\tau_F \frac{\partial F}{\partial t} = 1 - F, \tag{11}$$

$$\tau_D \frac{\partial D}{\partial t} = 1 - D. \tag{12}$$

The EPSC amplitude is modeled in Eq. (8) as the product of the initial EPSC amplitude A_0 with the facilitation factor F and the two depression factors D_1 and D_2. After each stimulating action potential, F is increased by a constant f [see Eq. (9)] while D is multiplied by a constant factor d [see Eq. (10)]. Between successive stimuli (i.e. arriving action potentials), F and D recover exponentially with time constants τ_F and τ_D, respectively [see Eqs. (11) and (12)]. D_1 and D_2 have different recovery rates. Note that, in contrast to the previous *FD*-residual calcium model, A_0 does not represent the release probability and is set equal to 1 in the simulations for simplicity.

2.3 Estimation of the non-parametric models of the four synapses

The estimation of the equivalent non-parametric (Volterra) models requires a broadband input, such as a random point-process input like a Poisson random impulse train (RIT), to probe fully the dynamics and the nonlinearities of the parametric models of the four synapses. The inter-pulse interval (IPI) of a Poisson RIT is a random variable with an exponential distribution whose mean value equals the inverse of the exponent. The first set of simulations used RIT inputs with data-record length of 400 input/output event pairs and a mean firing rate (MFR) of 2Hz (i.e., the IPI mean value is 500ms) covering an IPI range from 2 to 5,000ms, which is consistent with the physiological firing characteristics of many types of central neurons (Berger et al. 1988a; Barnes et al. 1990). This length of input/output data is adequate to obtain accurate kernel estimates of the respective non-parametric (Volterra) models following the methodology presented below. Note that it is necessary to increase the input–output data-record length to 2,000 event pairs in the case of the VC synapse. In a second set of simulations, Poisson RIT inputs of the same length as before and with various MFRs (from 0.5 to 100Hz) are used to simulate the four synaptic parametric models. The resulting input–output data are used to estimate the kernels of the respective non-parametric models in order to examine their ability to emulate the functional properties of the parametric models at these higher firing rates.

2.4 Volterra modeling and kernel estimation using Laguerre expansions

According to the theory of Volterra modeling, as adapted to the case of point-process inputs and contemporaneous varying-amplitude outputs (Volterra 1959; Marmarelis and Marmarelis 1978; Marmarelis 2004), the value of the output $y(t)$ of a nonlinear time-invariant system with finite memory M, can be represented at the time t_i by the following Poisson–Volterra (PV) model:

$$\begin{aligned} y(t_i) = k_1 &+ \sum_{t_i - M < t_j < t_i} k_2(t_i - t_j) \\ &+ \sum_{\substack{t_i - M < t_{j_1} < t_i \\ t_i - M < t_{j_2} < t}} \sum k_3(t_i - t_{j_1}, t_i - t_{j_2}) \\ &+ \sum_{\substack{t_i - M < t_{j_1} < t_i \\ t_i - M < t_{j_2} < t_i \\ t_i - M < t_{j_3} < t_i}} \sum \sum \sum k_4(t_i - t_{j_1}, t_i - t_{j_2}, t_i - t_{j_3}) + \ldots \end{aligned} \tag{13}$$

where k_1, k_2, k_3 and k_4 are the first, second, third and fourth order PV kernels of the system. The summations in Eq. (13) take place over all time of input events within a past epoch M (termed the "system memory") prior to t_i. These summations are constructed in a hierarchy of rising combinations of multiple preceding events. The first-order PV kernel, k_1, represents the amplitude of the EPSC attributed to a single input impulse (i.e., in the absence of any preceding input impulses within the memory extent M). The second-order PV kernel, k_2, represents the change in the EPSC amplitude caused by second-order interactions between the present input impulse and each of the past input impulses within the memory extent M. The third-order PV kernel, k_3, represents the change in the EPSC amplitude caused by third-order interactions between the present input impulse and any two (not necessarily different) preceding input impulses within M. The fourth-order PV kernel, k_4, represents the change caused by fourth-order interactions between the present input impulse and any three (not necessarily different) preceding input impulses within M and so on for higher-order kernels.

The form of these summations in Eq. (13) results from the reduced Volterra model (Marmarelis 2004), where one dimension of each kernel is collapsed because the input and output events are contemporaneous (they fall in the same event bin or have a constant delay), and the input single $x(t)$ is the following point-process (Poisson random sequence of action potentials):

$$x(t) = \sum_{i=1}^{N} \delta(t - t_i), \tag{14}$$

where $\delta(t - t_i)$ denotes the discrete impulse (Kronecker delta) at the time t_i, N is the total number of input–output events.

In order to facilitate the estimation of the PV kernels from broadband input–output data, we use the Laguerre expansion technique (Watanabe and Stark 1975; Marmarelis 1993; Song et al. 2007) which yields better estimates than the conventional kernel estimation technique of cross-correlation (Lee and Schetzen 1965; Sclabassi et al. 1988) and allows reliable kernel estimation from short and noisy datasets. This improved performance results from the utilization of the orthonormal basis of discrete-time Laguerre functions to expand the kernels and reduce the number of unknown parameters to be estimated.

According to this methodology, the ith-order PV kernel k_i is expanded in terms of L discrete-time Laguerre basis functions $b_j(\tau)$ as:

$$k_i(\tau_1,\ldots,\tau_{i-1}) = \sum_{j_1=1}^{L}\cdots\sum_{j_{i-1}=1}^{L} c_i(j_1,\ldots,j_{i-1})b_{j_1}(\tau_1)\ldots b_{j_{i-1}}(\tau_{i-1}), \quad (15)$$

where c_i are the kernel expansion coefficients. The PV model of Eq. (13) can be rewritten as:

$$y(t_i) = c_1 + \sum_{j=1}^{L} c_2(j)v_j(t_i) + \sum_{j_1=1}^{L}\sum_{j_2=1}^{L} c_3(j_1,j_2)v_{j_1}(t_i)v_{j_2}(t_i) + \sum_{j_1=1}^{L}\sum_{j_2=1}^{L}\sum_{j_3=1}^{L} c_4(j_1,j_2,j_3)v_{j_1}(t_i)v_{j_2}(t_i)v_{j_3}(t_i) + \ldots, \quad (16)$$

where

$$v_j(t) = \sum_{t-M<t_i<t} b_j(t-t_i), \quad (17)$$

$$b_j(\tau) = \begin{cases} (-1)^{\tau}\alpha^{(j-\tau)/2}(1-\alpha)^{1/2}\sum_{k=0}^{\tau}(-1)^k\binom{\tau}{k}\binom{j}{k}\alpha^{\tau-k}(1-\alpha)^k & (0\le\tau<j) \\ (-1)^{j}\alpha^{(\tau-j)/2}(1-\alpha)^{1/2}\sum_{k=0}^{j}(-1)^k\binom{\tau}{k}\binom{j}{k}\alpha^{j-k}(1-\alpha)^k & (j\le\tau\le M) \end{cases}. \quad (18)$$

The Laguerre parameter α ($0 < \alpha < 1$) determines the rate of exponential asymptotic decline of the Laguerre basis functions and in practice is selected through successive trials so that the prediction mean-square error is minimized. The utilization of basis functions for kernel expansion improves the kernel estimation because it reduces the number of free parameters to be estimated from the data (since the number L of basis functions is typically much smaller than the number M of samples within the system memory, i.e., the length of each kernel dimension.

The unknown kernel expansion coefficients c_i are estimated through least-squares fitting of the input–output data in Eq. (15) using singular value decomposition to avoid numerical instabilities. A 1ms bin size is used to generate the discrete Laguerre basis functions. The obtained estimates of the expansion coefficients can be used to construct the PV kernel estimates according to the Eq. (15).

The prediction accuracy of the obtained PV models was evaluated with the computed out-of-sample normalized root mean-square error (NRMSE) of the output prediction:

$$\mathrm{NRMSE} = \left(\frac{\sum_{i=1}^{N}(y(t_i)-\hat{y}(t_i))^2}{\sum_{i=1}^{N}y(t_i)^2}\right)^{1/2} \quad (19)$$

where $\hat{y}$ is the output predicted by the estimated PV model for a novel RIT input different from the one used for kernel estimation, y is the output of the respective parametric synapse model for the novel RIT input. The use of different RIT inputs for kernel estimation and prediction evaluation is necessary to avoid overfitting the PV kernels/model to the data.

The number of basis function (L) and the Laguerre parameter α are optimized using the criterion of out-of-sample NRMSE. For a given model order, optimal α is searched in the range of (0, 1) for increasing L. The combination of α and L that gives the smallest out-of-sample NRMSE is chosen to construct the PV kernels.

2.5 PV kernels and response descriptors

Each of the aforementioned PV kernels quantifies interactions of a specific number of preceding input impulses that is determined by its order. However, a certain number of preceding input impulses (within the epoch of system memory) make contributions to the output through all the PV kernels of the system. For instance, a single preceding impulse makes a contribution through the second-order PV kernel (k_2) but also through *all other* higher-order PV kernels present in a specific system. In other words, k_2 is not the same paired-pulse facilitation/depression function measured through the popular paired-pulse stimulation protocol.

To examine the effects of a given number of preceding input impulses within the epoch of system memory, we introduce the notion/measure of "response descriptors" (RD). The *i*th-order RD, r_i, exclusively represents the *i*th-order modulatory effect of any *i*-1 *different* preceding input impulses on the present output. There exist simple mathematical relations between the PV kernels and the *i*th-order RD. For instance, in the case of a third-order PV model (Fig. 2):

$$r_1 = k_1 \tag{20}$$

$$r_2(\tau) = k_2(\tau) + k_3(\tau, \tau) \tag{21}$$

$$r_3(\tau_1, \tau_2) = 2k_3(\tau_1, \tau_2) \tag{22}$$

Note that, for a triplet of input impulses, the output is given by:

$$y(\tau_1, \tau_2) = r_1 + r_2(\tau_1) + r_2(\tau_2) + r_3(\tau_1, \tau_2) \tag{23}$$

where $y(\tau_1, \tau_2)$ is the output predicted by the third-order PV model for the two preceding input impulses with time lags from the present output τ_1 and τ_2, respectively (see Fig. 2E). This mathematical formalism can be extended to any order of PV model. Equations (20)–(23) show that the set of PV kernels and the set of RDs are equivalent in terms of output prediction. The RDs will be used for illustration of the results in this paper and for their comparative evaluation vis-a-vis previously reported results on synaptic STP, because they more closely relate to the established notion of paired-pulse facilitation/depression. An illustrative example of PV kernels and RDs for a third-order PV model obtained from the simulated data of the parametric *FD* model of the SC synapse is shown in Fig. 2. Similarly, the RDs of a fourth-order PV kernel model can be expressed as (Fig. 7):

$$r_1 = k_1 \tag{24}$$

$$r_2(\tau) = k_2(\tau) + k_3(\tau, \tau) + k_4(\tau, \tau, \tau) \tag{25}$$

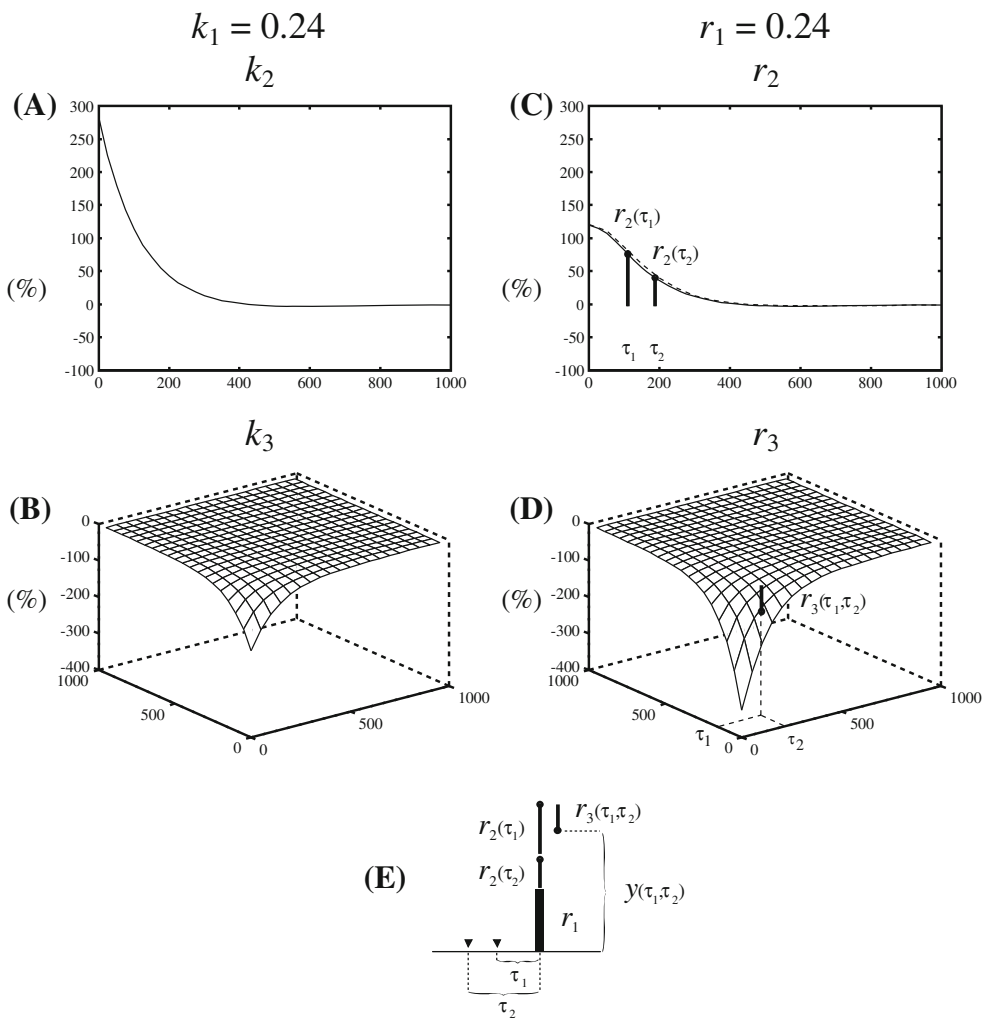

Fig. 2 The Poisson-Volterra (PV) kernels and corresponding response descriptors (RDs) of the third-order PV model of the SC synapse. (**A**) The second-order PV kernel k_2 representing the second-order interactions with a preceding impulse (exhibiting facilitation in this case), where the abscissa axis is the inter-pulse interval (IPI) values of the preceding impulse. (**B**) The third-order PV kernel k_3 representing the third-order interactions with two preceding impulses (exhibiting depression in this case), where the two abscissa axes are the IPI values of the two preceding impulses. (**C**) The second-order RD r_2 that is equal to the paired-pulse response function. (**D**) The third-order RD r_3 that can be viewed as the triple-pulse response function. The separation of paired-pulse facilitation and depression characteristics is evident in (**C**) and (**D**), respectively. (**E**) The response to a three-pulse stimulus with IPIs τ_1 and τ_2 is the summation of r_1, $r_2(\tau_1)$, $r_2(\tau_2)$ and $r_3(\tau_1, \tau_2)$

$$r_3(\tau_1,\tau_2) = 2k_3(\tau_1,\tau_2) + 3k_4(\tau_1,\tau_1,\tau_2) + 3k_4(\tau_2,\tau_2,\tau_1) \quad (26)$$

$$r_4(\tau_1,\tau_2,\tau_3) = 6k_4(\tau_1,\tau_2,\tau_3) \quad (27)$$

and it can be proven that,

$$y(\tau_1,\tau_2,\tau_3) = r_1 + r_2(\tau_1) + r_2(\tau_2) + r_2(\tau_3) + r_3(\tau_1,\tau_2) + r_3(\tau_1,\tau_3) + r_3(\tau_2,\tau_3) + r_4(\tau_1,\tau_2,\tau_3) \quad (28)$$

The RDs may also be directly estimated from the input–output data with separate consideration of each output with respect to the number of impulses within its memory. However, the current method is computationally more convenient since the estimation of PV kernels only involves combinations of v instead of the combinations of impulses in the system memory (M).

3 Results

The parametric models of the aforementioned four synapses (SC, PF, CF and VC) are simulated for the parameter values shown in Table 1 and Poisson RIT inputs with MFR of 2Hz. Using the resulting synthetic input–output data, we estimate the PV kernels of the corresponding non-parametric models employing the methodology described in the previous section.

A Volterra kernel model is expressed as a functional power series of input with progressively higher-order kernels capable of describing higher-order nonlinear dynamics. Theoretically, it can replicate arbitrary system nonlinearity. However, the number of coefficients to be estimated grows exponentially with increases in model order, and thus makes it impractical to keep all the high order terms. So in practice, the first issue in kernel estimation is to find out how many terms (orders) are needed for accurate replication of the system nonlinearity and then to truncate the unnecessary high order terms. This is typically done using statistical model order selection criteria (MOSC) (Marmarelis 2004). However, existing noise-based statistical MOSCs are not applicable to the problem in this study since the modeled systems (parametric models) are noise-free. The residual errors are purely due to the difference between the kernel model and the parametric model, and their statistical significance thus can not be evaluated using statistical criteria. Therefore, we choose to use a simple and straightforward model order selection approach in this study: if the residual error (NRMSE) is below a certain level (5%) for a given model order, the model is considered a "practically complete" (as opposed to "mathematically complete") model since the majority of the system nonlinearity is accounted for.

We estimate first, second, third and fourth order PV models of the four synapses. The out-of-sample NRMSEs of model predictions are given in Table 2. The first-order kernel model is a scalar, which is equal to the mean of output amplitudes. No nonlinear dynamic is included and its model predictions are constant. However, the NRMSEs of first-order kernel models show that all four synapses have strong output nonlinearities given the unitary input amplitudes. The second, third and fourth-order kernel models are capable of modeling up to second, third and fourth-order nonlinear systems, respectively. In PF, CF and VC synapses, most of the NRMSEs are diminished (<5%) when the model order is increased to two; in SC synapse, there is still a large portion of residual error in the second order kernel model. The model order should be increased to three to obtain a NRMSE below 5%. These results show that for Poisson random inputs with a 2Hz MFR, PF, CF and VC are primarily second-order nonlinear systems, whereas the SC synapse is a third-order nonlinear system, given the order of the system is defined as the order of the systems nonlinearity.

3.1 Estimated PV kernels for the parametric models of the four central synapses

The four synapses included in this paper show different forms of STP. This could be revealed by a simple, fixed-interval train (FIT) simulation (Fig. 3). For instance, during a 100Hz train (10 pulses), the EPSC amplitudes of SC synapse peak at the second impulse and then decline in the rest of the impulses; the EPSC amplitudes of PF synapse keep increasing from the second impulse to the fourth impulse and then plateau; whereas in both CF and VC synapses, EPSC amplitudes monotonically decline. This FIT simulation only shows the behavior of the synapses with respect to 10ms intervals. In the kernel models estimated with random-interval trains, the four different forms of STP are fully quantified with respect to arbitrary IPIs and explicitly visualized in the kernels. To make the kernel results comparable, third-order PV kernel models are

Table 2 The NRMSEs of the estimated PV models for the four types of synapses (using the parameter values in Table 1) for Poisson RIT inputs different from the ones used for PV kernel estimation

Model order	SC	PF	CF	VC
1st	27.98	40.27	13.1	32.72
2nd	15.32	3.82	4.82	4.35
3rd	4.72	0.27	2.36	3.66
4th	1.89	0.21	1.74	2.23

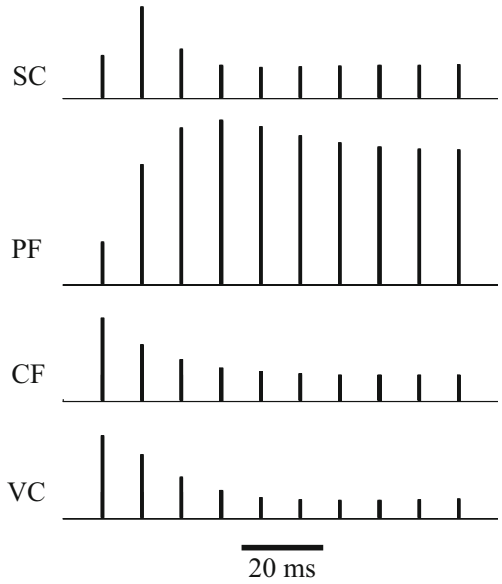

Fig. 3 The EPSC responses simulated with the parametric models of the four synapses for a fixed-interval input train of ten impulses (IPI of 10 ms or 100 Hz)

used in all four synapses. These models precisely predict the outputs of the synapses for 2Hz Poisson random inputs (Fig. 4).

3.1.1 SC synapse

Figure 2 and the first column of Fig. 5 shows the estimated RDs for the third-order non-parametric model of the SC synapse. The first-order RD (r_1) is equal to the initial release probability of the synapse ($r_1 = k_1 = F_1 = 0.24$). The second-order RD, $r_2(\tau)$, represents the modulatory effect of a single preceding impulse upon the present response as a function of the IPI value τ. It is seen that this effect is positive (i.e., facilitatory) for all IPI values up to about 400ms, diminishing for larger IPI values. Maximum second-order facilitation is observed for the shortest IPI and it is less than half the respective value of the second-order PV kernel, $k_2(\tau)$, that does not take into account the depressive effect of third-order dynamics (represented by $k_3(\tau, \tau)$, which is solely depressive for this synapse; see Fig. 2(A) and (C) for comparison). Note that $r_2(\tau)$ depends on k_2 (τ) and $k_3(\tau, \tau)$, according to Eq. (21) and its maximum value at the shortest IPI (120%) matches the maximum paired-pulse facilitation ratio in the parametric model of the SC synapse ($\rho - 1 = 1.2$; Fig. 2(C). The third-order RD, $r_3(\tau_1, \tau_2)$, describes the joint contribution of two preceding impulses to the present response as a function of the two IPI intervals τ_1 and τ_2. It is shown to be solely depressive [with double the values of the third-order PV kernel, according to Eq. (22); see Fig. 2(B) and (D) for comparison] with the most negative value at the shortest IPI interval being almost three times the value of k_1. This result shows that the SC synapse has a strong depressive third-order nonlinearity. For an input of three impulses, e.g., the first three impulses in the 100Hz FIT (Fig. 3, first row), the response $y(\tau_1, \tau_2)$ to the most recent impulse (termed "present") is facilitated by the positive second-order contributions of each preceding impulse, $r_2(\tau_1)$ and $r_2(\tau_2)$, and depressed by the negative third-order joint contribution of the two preceding impulses $r_3(\tau_1, \tau_2$; Fig. 2E). When the absolute value of $r_3(\tau_1, \tau_2)$ is larger than $r_2(\tau_2)$, the third response becomes smaller than the second response and forms a peak in the second response, which is precisely what happens in the 100Hz FIT (Fig. 3, first row). The estimated PV kernels and the corresponding RDs, r_2 and r_3, fully quantify the effects of paired-pulse facilitation and triple-pulse depression for arbitrary IPIs in SC synapses.

The small prediction errors imply accurate estimation of the PV kernels and RDs. In addition, the estimated RDs are also directly validated with the RDs numerically calculated through the parametric model. The estimated r_2 and r_3 well approximate the actual r_2 (Fig. 2(C), dashed line) and r_3 (not shown) with arbitrary IPIs.

3.1.2 PF synapse

The second column of Fig. 5 shows the obtained results for the PF synapse. As indicated for the SC synapse model, r_1 ($=k_1$) is equal to the initial release probability ($F_1 = 0.05$), which is smaller than that of the SC synapse. The obtained RDs for the PF synapse have similar qualitative characteristics with the SC synapse, i.e. r_2 is positive for all IPIs (solely facilitatory) and r_3 is negative for all IPIs (solely depressive). However, the magnitude of r_2 is much larger than that of the SC synapse because of the much higher

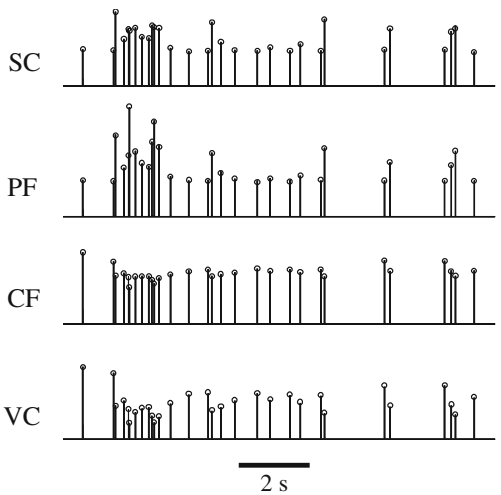

Fig. 4 The EPSC responses simulated with the parametric models of the four synapses (*bars*) for a Poisson random-interval train (RIT) input with 2 Hz mean firing rate (MFR), and the predictions of the third-order PV models (*circles*) accurately replicating the four different forms of STP

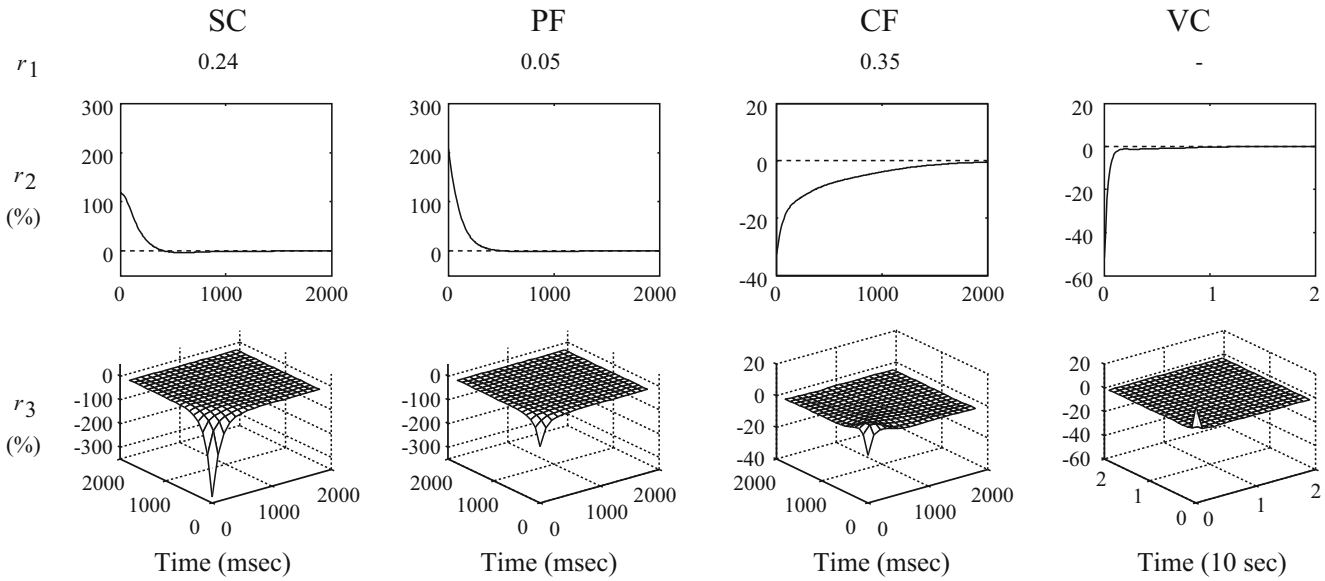

Fig. 5 The estimated RDs of the four types of synapses. Each column shows the RDs of one type of synapse. Note that in the SC, PF and CF synapses, r_1 is equal to the initial release probability, but in the VC synapse, r_1 is equal to unity by definition and thus not shown

paired-pulse facilitation ratio in the PF synapse (ρ = 3.1). Also, the magnitude of r_3 becomes much smaller compared to that of the SC synapse model. This confirms the NRMSE result showing that the majority of the PF synapse nonlinearity is of second order (Table 2). In a triple-pulse train, e.g., the first three impulses in the 100Hz FIT (Fig. 3, second row), the third response $y(\tau_1, \tau_2)$ is strongly facilitated by the second-order contributions of each of the preceding impulses, $r_2(\tau_1)$ and $r_2(\tau_2)$, and only weakly depressed by the negative third-order joint contribution of the two preceding impulses $r_3(\tau_1, \tau_2)$. The train thus shows a nearly monotonic-increasing pattern.

3.1.3 CF synapse

The third column of Fig. 5 shows the obtained results for the CF synapse. The value of r_1 is equal to the initial release probability 0.35, which is larger than in the previous two synapses. The values of r_2 are negative for all IPIs, and they are smaller in absolute value than the previous two synapses. The values of r_3 are also negative and small relative to r_2, indicating that the second-order nonlinearities are dominant in the CF synapse, as in the case of the PF synapse. Contrary to the SC and PF synapses, the CF synapse shows negative r_2 values that quantify the depressive effect of each preceding impulse upon the present response as a function of the IPI. The absolute values of r_2 decline rapidly for IPI < 140ms and more slowly for longer IPIs until they diminish around 2,000ms, indicating that we cannot fit the waveform of r_2 with a simple exponential function. We also observe that the form of r_3 is biphasic, crossing from negative (depressive) to positive (facilitatory) values around IPI of 100ms. The peak value of r_2 (−35% at the minimum IPI) is equal to the initial release probability of this synapse.

3.1.4 VC synapse

Similar to the CF synapse, the VC synapse has a dominant second-order suppressive kernel/RD (Fig. 5, fourth column). However, unlike the CF synapse, the small values of r_3 are positive for the VC synapse. Note that r_1 (not plotted) is equal to A_0 (=1), which is defined as the baseline response amplitude in the FD_1D_2 model. We observe that the waveform of r_2 is comprises of an early fast-recovering component that is strongly negative and a subsequent slow-recovering component that has weaker negative values. This result shows that the two depressive components (D_1 and D_2 in Eq. 8) in the parametric model of the VC synapse are captured by the second-order kernel of the non-parametric PV model. The facilitation determined by F in the parametric model of the VC synapse is masked by D_1 and D_2 in r_2, since the overall effect of D_1, D_2 and F is suppressive. The small values of r_3 indicate that the nonlinearity of the VC synapse is primarily of second order.

3.2 Interpretation and comparison of the non-parametric models of the four synapses

The first three synapses (SC, PF and CF) share the same parametric model structure but have different parameter values. The corresponding non-parametric PV kernel models provide an elucidating way to appreciate how the key model parameters affect the input–output transforma-

tional properties of each synapse (Fig. 5). For instance, the nonlinearities of the PF synapse are primarily determined by the residual calcium-dependent facilitation mechanism. The depression mechanism is relatively weak due to the fact that PF synapse has a very small initial release probability (0.05) which limits the depression caused by vesicle depletion. These are reflected by the prominent positive r_2 and relatively small negative r_3. By contrast, the SC synapse has a much higher initial release probability (0.24) which causes a higher level of depletion, leading to larger negative values of r_3, i.e., in a triple-pulse train, the joint contribution of pairs of preceding impulses (exclusive of their second-order contributions) to the present output becomes strongly negative because of the small number of available vesicles after two consecutive releases. Nonetheless, the modulatory effect of each single preceding impulse is still facilitatory (as indicated by the positive values of r_2).

The CF synapse lacks the facilitation mechanism (Dittman et al. 2000). In its *FD* model, the *F* factor remains constant through time regardless of the input pattern (Table 1). Its nonlinearity is exclusively determined by the kinetics of recovery from vesicle depletion which is significant due to the high initial release probability (0.35), thus its r_2 values are negative. Negative also are the r_3 values for short IPIs, but become slightly positive for IPIs longer than about 100ms.

The VC synapse has a different parametric model structure involving two depression factors in addition to the facilitation factor. The respective non-parametric PV model provides a general representation of its input–output transformational properties and makes it possible to assess the functional similarities and differences with the different STP characteristics of the other three types of synapses—even though the latter have different forms of parametric models. The main distinguishing characteristic of the parametric VC synapse model is its double-component depression (D_1 and D_2) which results in a double-exponential shape for r_2 (with time courses approximately matched by the time-constants τ_{D1} and τ_{D2} given in Table 1). The fast facilitation factor (*F*) of the parametric model of the VC synapse is reflected on the positive values of r_3. Note that the *FD* model of the CF synapse also yields a double-exponential shape for r_2 (see third column of Fig. 3) which is due to the residual calcium-dependent recovery of depletion, resulting in different recovery rates for different IPIs—i.e. when the IPI is short, the residual calcium caused by a preceding impulse has a high concentration and results in a fast recovery rate; while for long IPIs, the residual calcium decays to lower levels that result in a slow recovery rate. This mechanism is modeled differently in the two parametric models but its effects on the STP are represented similarly in the respective non-parametric models, assisting the comparison of their functional characteristics.

In summary, the results above show that each form of synaptic STP has its own characteristic pattern that is reflected quantitatively on the shapes, polarities and time durations of its PV kernels and corresponding RDs. It is evident that the PV kernels and the corresponding RDs contain quantitative and biologically interpretable information about the dynamics and nonlinearities underlying the STP processes in these four types of synapses.

3.3 Higher-order PV models for higher input firing rates

It is shown above that, for Poisson RIT inputs with MFR of 2Hz, the third-order PV models are able to highly accurately predict the outputs of all four types of synapses. For such inputs, the IPI values are random independent samples drawn from an exponential distribution with mean value of 500ms. In this study, we use an absolute refractory period of 2ms and the IPI values are generated in the range of 2–5,000ms. The importance of using Poisson RIT input is that it includes many of the temporal patterns typical of CNS synapses in physiological conditions. The MFR of 2Hz is selected on the basis of the firing characteristics of many central neurons, e.g., hippocampal CA1 and CA3 neurons of free-moving rats (Berger et al. 1983; Barnes et al. 1990; Deadwyler et al. 1996). However, different firing characteristics with higher or lower average rates and/or different distributions also exist. The effect of the different firing rates on the obtained PV models is discussed further in this section.

In order to examine the effect of higher firing rates on the efficacy of the non-parametric modeling approach, we simulate the parametric models with inputs of higher MFRs and estimated the respective PV kernels to examine the predictive capabilities of the resulting non-parametric models for these input characteristics. The PV kernels of the parametric models of the SC, PF and CF synapses are estimated with data obtained from Poisson RIT inputs with various MFRs in the range of 0.5–100Hz. Because of their random character, these inputs contain practically all possible input sequences that can naturally occur under physiological conditions. Figure 6 shows the prediction NRMSE of the estimated PV models of various orders (from first to fourth order) for the various input MFRs. The NRMSE of the first-order PV model quantifies the average output variations around the mean response of the synapses for each input MFR and can be used as a baseline to judge the performance of the higher-order PV models. In the case of the PF and CF synapses, it is seen that the second-order PV models can account for a significant portion of the output variations and the third-order PV models can predict the outputs very well over the entire range of input MFRs (up to 100Hz) with the fourth-order PV models offering insignificant improvement. In the SC synapse, the second-

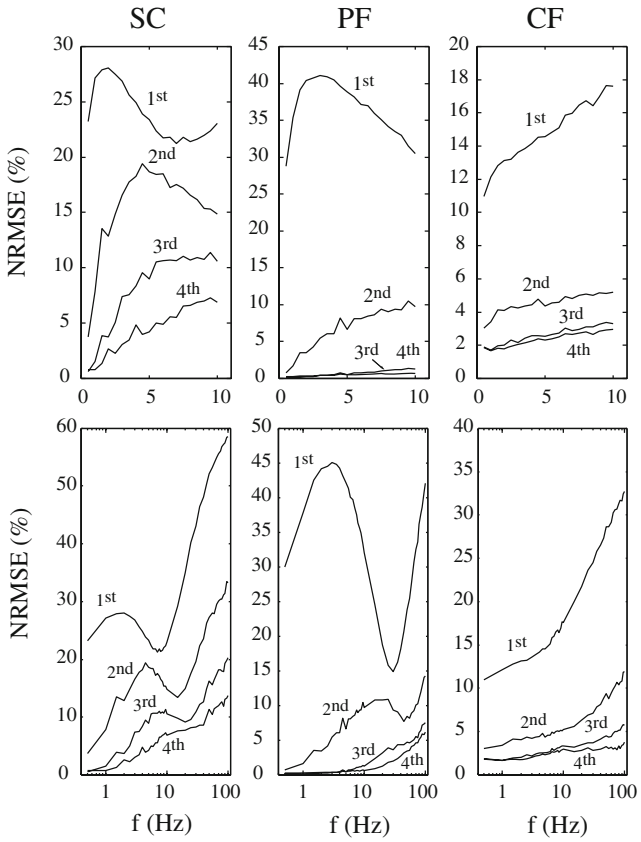

Fig. 6 Predictive accuracies of the non-parametric PV models of three types of synapses (SC, CF, PF) for various MFRs of the RIT input. *Upper panel*: input MFRs in the range of 0.5–10 Hz. *Lower panel*: input MFR in the range of 0.5–100 Hz (plotted in log scale)

order PV model gave poor predictions for MFRs higher than 1Hz, as already indicated in the results of the 2Hz MFR presented above, but the NRMSE of the third-order PV model was reduced to levels below 5% for MFRs up to 2Hz (as shown above) and remained below 10% for MFRs less than 30Hz. The NRMSE of the third-order prediction increased significantly for MFRs larger than 30Hz, reaching almost 20% for the maximum MFR of 100Hz. The use of a fourth-order PV model reduced the NRMSE further, keeping it below 5% for MFRs up to 6Hz and below 10% for MFRs less than 50Hz. A steady increase of the fourth-order prediction NRMSE with increasing input MFR is observed that indicates the need for even higher-order PV kernels to capture better the system nonlinearities and improve the model prediction for higher input MFRs.

Figure 7 shows the PV kernels and RDs of the fourth-order PV model of the SC synapse estimated with a Poisson RIT input of 2Hz MFR. The fourth-order term (k_4/r_4) in the fourth-order PV kernel model contributes to the prediction of the outputs with more than two preceding input impulses. For example, for a quad-pulse train (Fig. 7G), the fourth output is predicted by the fourth-order PV kernel model as the summation of the first-order term contributed by the present impulse (r_1), second-order terms from each preceding impulse [$r_2(\tau_1)$, $r_2(\tau_2)$ and $r_2(\tau_3)$], third-order terms contributed by each pair of preceding impulses [$r_3(\tau_1, \tau_2)$, $r_3(\tau_1, \tau_3)$ and $r_3(\tau_2, \tau_3)$] and the fourth-order term jointly determined by all three preceding impulses [$r_4(\tau_1, \tau_2, \tau_3)$, Fig. 7G]. k_4 and r_4 are positive 3D matrices ($M \times M \times M$) with peak value at minimum intervals. They allow the fourth-order model to more accurately capture the systems nonlinearities associated with more-than-two preceding impulses in the system memory window.

In the fourth-order PV model, the estimated k_1 was the same as that of the third-order PV model, while k_2 and k_3 were different from those of the third-order PV model (compare Figs. 2 and 7). This is due to the fact that both PV models are mathematically incomplete as shown in their residual errors, although they are practically complete according to the chosen NRMSE threshold (5%). In mathematically incomplete PV models, the extra high order terms, e.g., k_4 in the fourth-order PV model of the SC synapse, are nonzero. These high order terms project to the lower-order PV kernels (k_2 and k_3) of the lower-order PV models, e.g., the third-order PV model of the SC synapse in this case, and make these lower-order PV kernels (k_2 and k_3) different in the two models. Direct comparison of the PV kernels is generally non-informative in the mathematically incomplete PV models of different model orders. By contrast, the PV kernels of the mathematically complete models do not change as the model order changes since these PV models have the same non-zero terms and the additional higher-order PV kernel in the higher-order PV model will not interfere with the lower-order PV kernels since they are equal to zero. However, it is remarkable that the RDs of the two practically complete PV models are nearly identical (Figs. 2 and 7). Such favorable property of the RD representation can be explained as the following: as shown in the Method section, RDs, which are derived from the PV kernels, have a simple interpretation, i.e., the *i*th-order RD, r_i, exclusively represents the *i*th-order modulatory effect of any *i*-1 *different* preceding input impulses on the present output. *i*th-order RD thus does not contribute to the prediction of the responses with *i*-1 or fewer impulses. When the MFR of the Poisson random input is low, the probability of having many input impulses in the modeled system's memory window (M) is small. The majorities of the input patterns (isolated by intervals larger than M) are single impulses, pairs and triplets. Practically complete models, e.g., third and fourth-order PV models of SC synapse, achieve low NRMSE mainly by accurately predicting those commonly encountered patterns. The first, second and third-order RDs, which correspond to the prediction of single impulses, pairs and triplets respectively, are all very close to their true values (as indicated by the small NRMSE and validated by the direct calculation) and

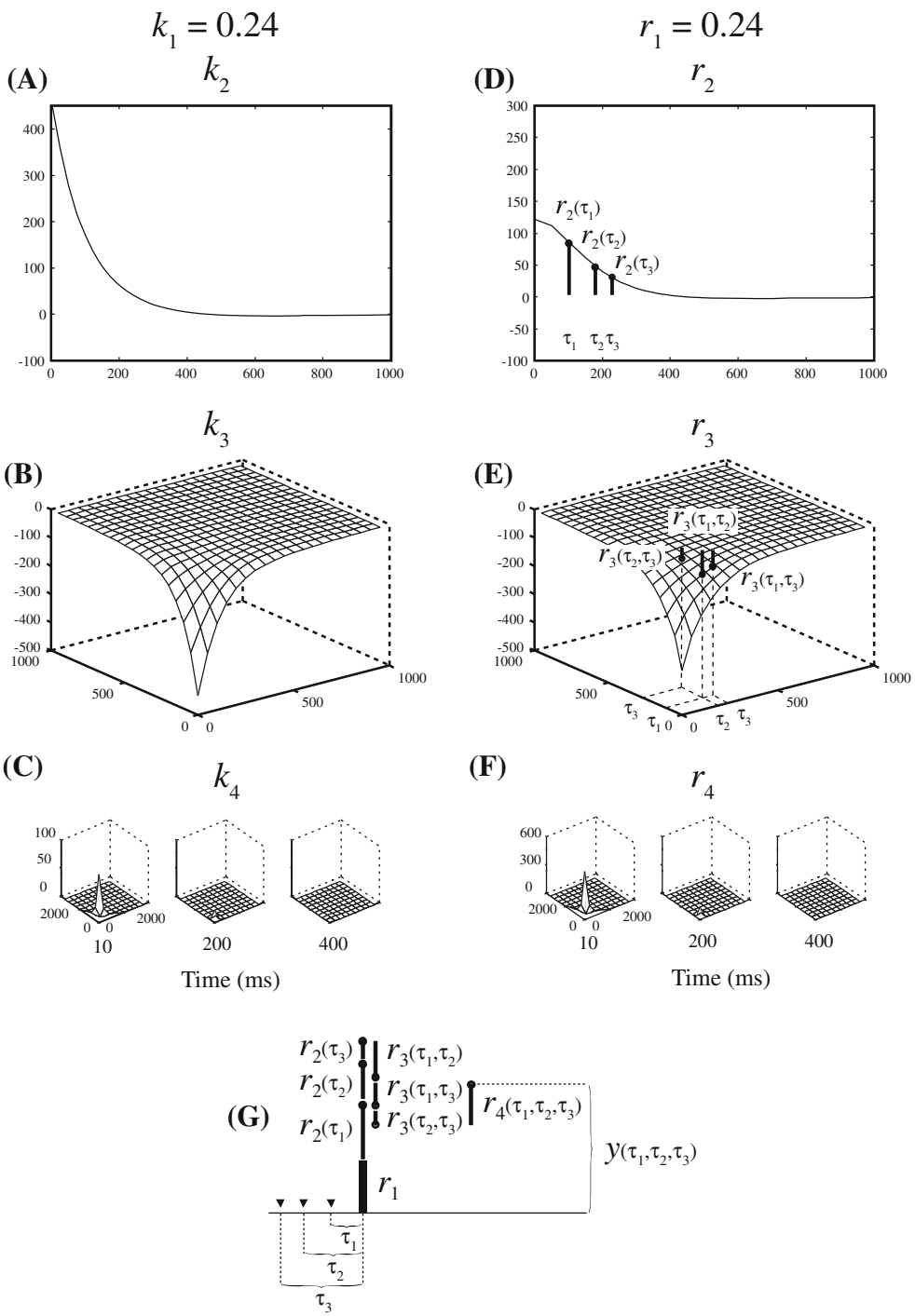

Fig. 7 The PV kernels and corresponding RDs of the fourth-order PV model of the SC synapse. (**A**) The second-order PV kernel k_2. (**B**) The third-order PV kernel k_3. (**C**) Slices of the fourth-order PV kernel k_4 at three selected lags (from 10 to 400 ms). (**D**) The second-order RD r_2. **E** The third-order RD r_3. (**F**) Slices of the fourth-order RD r_4 at three selected lags (from 10 to 400 ms). (**G**) RD contributions to the present output

therefore remain stable across different model orders. In the PV kernel representation, by contrast, *i*th-order PV kernel also contributes to the predictions of the responses with *i*-1 or fewer impulses. The estimates of the lower-order PV kernels, e.g., k_2 and k_3, are thus altered by the inclusion of higher-order PV kernels and consequently show different values across different model orders.

Figure 8 shows the changes in the RDs of first, second and third order that are based on the PV kernel estimates of the second, third and fourth-order PV models of the SC synapse, obtained for various values of input MFR in the range from 0.5 to 10Hz. The obtained r_1 values show a significant dependence on input MFR for the second-order model, but no significant dependence for the fourth-order model. For the third-order model, which was selected for the main stimulation protocol with MFR of 2Hz, the dependence of the r_1 values on the input MFR is significant only for MFR > 4Hz. The obtained r_2 values exhibited a

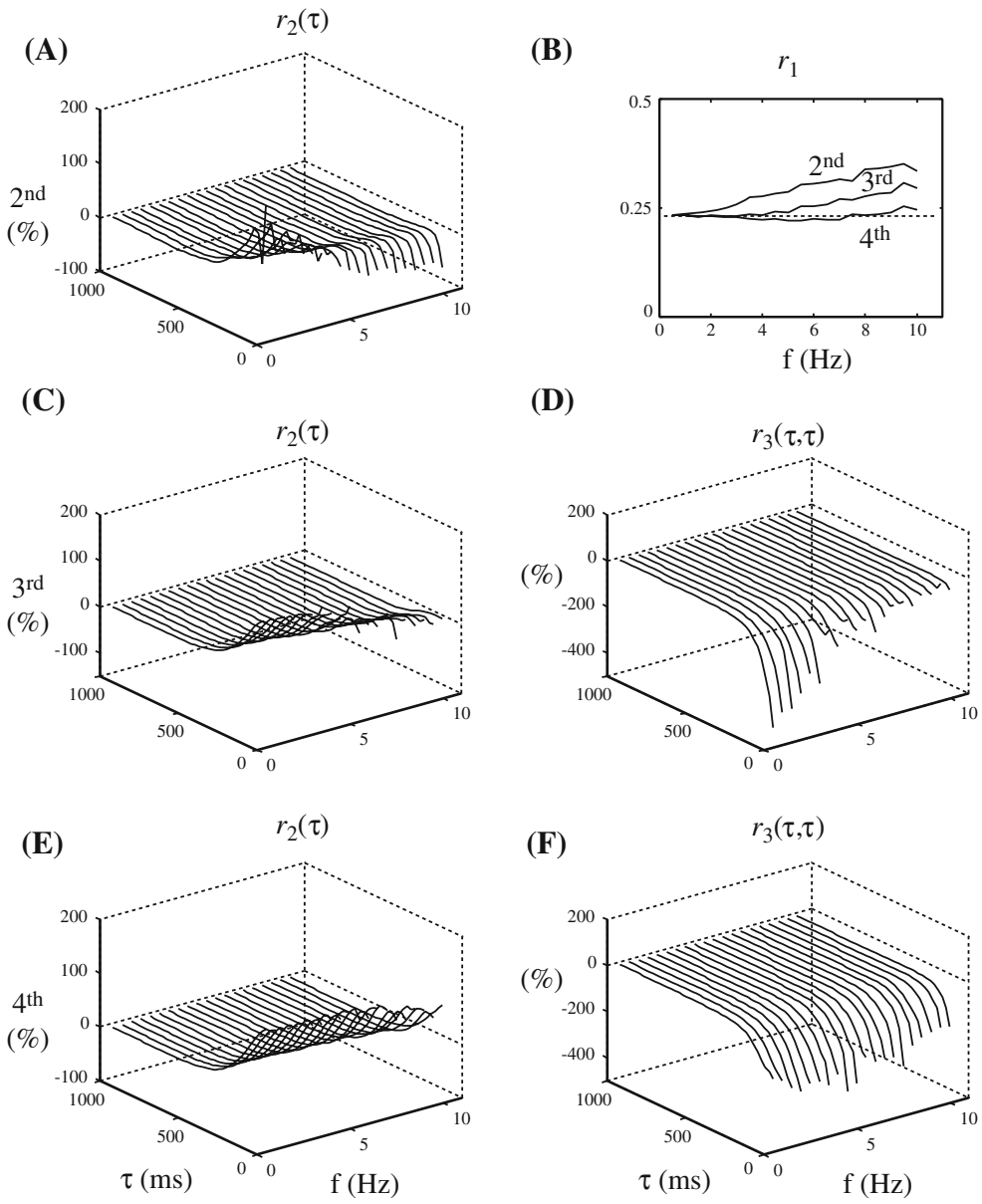

Fig. 8 The dependence of the RDs of the SC synapse on the input MFR and PV model order. (**A**), (**C**) and (**E**) The second-order RD r_2 for the second, third and fourth order PV models as a function the input MFR *f*. (**B**) The first-order RD r_1 for the second, third and fourth order PV models as a function the input MFR *f*. (**D**) and (**F**) The diagonal slice of the third-order RD r_3 for the third and fourth order PV models as a function the input MFR *f*. Note that r_1, r_2 and r_3 are less variant with changing input MFR for the fourth order PV model

strong dependence on input MFR for the second-order PV model, changing from positive to negative values around 3Hz. Significant dependence was also observed for the third-order PV model when MFR was higher than 4Hz, but no significant dependence was observed in the case of the fourth-order PV model for MFR up to 8Hz. The obtained r_3 values exhibited a strong dependence on input MFR for the third-order PV model (especially for MFR > 3Hz), but less dependence for the fourth-order PV model. These results show that the kernel estimates and the corresponding RDs of higher-order PV models not only provide better output predictions as indicated in the NRMSE results, but also are more robust to the changes of input MFR. When the input MFR is further increased (e.g., higher than 15Hz), significant changes occur even for the fourth-order PV model (not shown), indicating that higher-order models are needed to fully represent the system dynamic nonlinearities in this higher firing rates.

In addition to the input characteristics (e.g., MFR), the other determinant of the required model order, obviously, is the system nonlinearity to be modeled. For example, for a second-order nonlinear system, no matter how the MFR is enhanced, second-order PV model will always be complete. The number of impulses in the system memory window only provides the upper-bound of the required model order. This is shown in the PF synapse models (Fig. 9). The second order kernel model of PF synapse was constant in the range of 0.5–5Hz showing that in this range, PF synapse could be sufficiently characterized as second-order nonlinear system; the third and fourth order kernel models

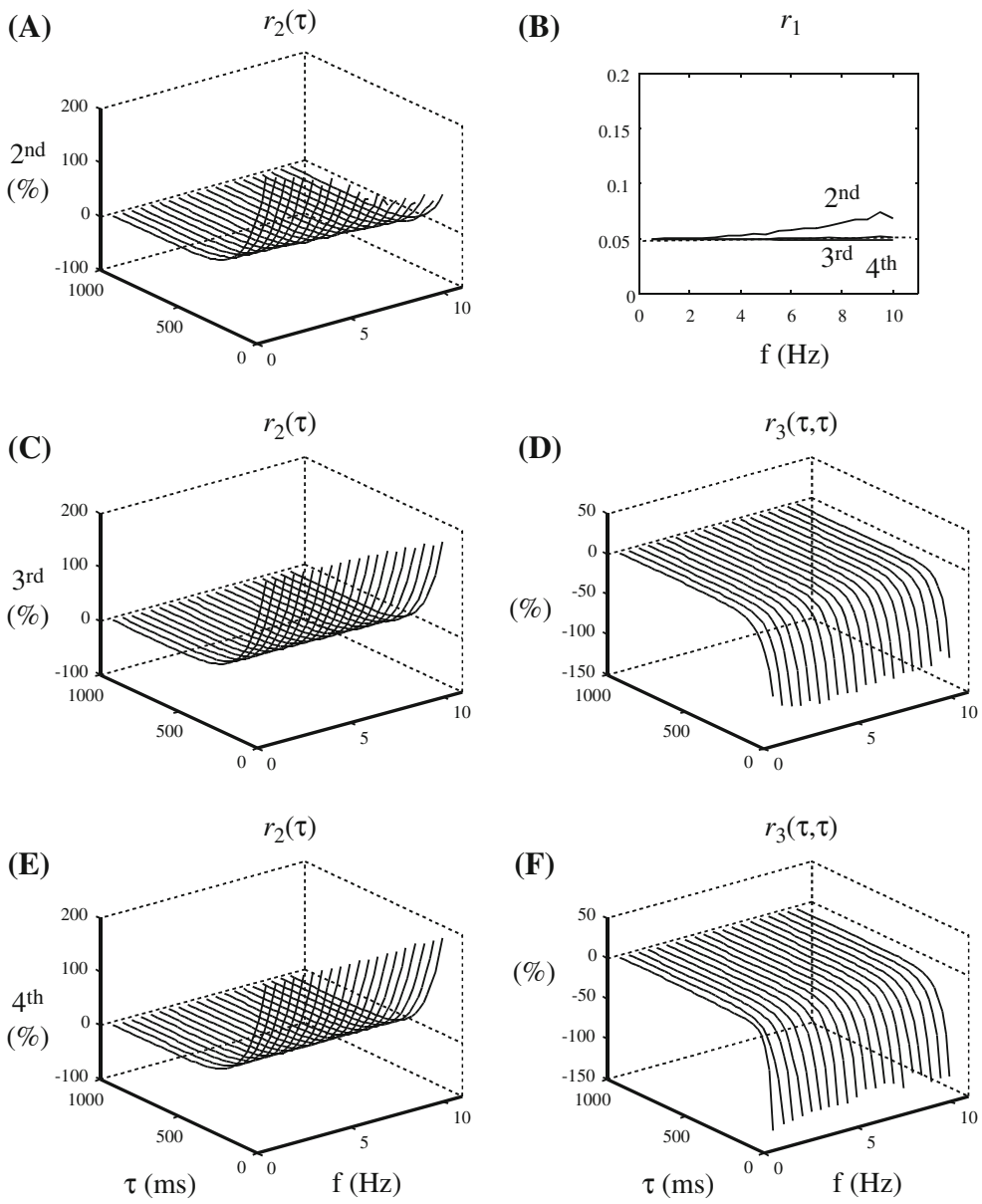

Fig. 9 The dependence of the RDs of the PF synapse on the input MFR and PV model order. (**A**), (**C**) and (**E**) The values of r_2 from the second, third and fourth order PV models for different Poisson input MFRs. (**B**) The values of r_1 from the second, third and fourth order PV models for different Poisson input MFRs. (**D**) and (**F**) Diagonal slice of r_3 from the third and fourth order PV models for different Poisson input MFRs. No significant dependence is observed for the third and fourth order model, indicating completeness of the PV model for input MFR up to 10 Hz

were constant in the whole range of 0.5–10Hz indicating that in this broader range, third-order model was sufficient. This result shows that the PF synapse is intrinsically less nonlinear than the SC synapse, in the sense that for a given input range, it can be fully characterized by lower-order kernel models.

In summary, the required model order to adequately characterize a system is jointly determined by both the input characteristics and the intrinsic system nonlinearity. Higher-order kernel models are more complete and robust to the change of input characteristics (e.g., MFR) in general. RDs of practically complete models are insensitive to the model order and thus are more appropriate for representations and interpretations of the system nonlinearity.

4 Discussion

In this paper, we applied a general, non-parametric modeling approach to the study of STP in CNS synapses. In this approach, the input–output transformational properties of various synapses are probed with broadband stimuli (Poisson RITs). The synaptic nonlinearities, associated with STP, are represented by non-parametric models utilizing PV kernels estimated from input–output data, which characterized fully the transformation of the presynaptic sequence of impulses into the postsynaptic EPSCs. Using a recently developed technique, the PV kernels can be accurately and reliably estimated from short input–output datasets. In the first half of this paper, we estimated the PV kernels using the input–output data simulated with established parametric

models of several CNS synapses for Poisson random impulse trains (RITs) with MFR of 2Hz. It was found that third-order PV models (involving first, second and third-order PV kernels) could predict accurately the outputs of these parametric synapse models to novel input patterns (so long as the MFR did not exceed significantly 2Hz). The nonlinear dynamics defined by the specific mathematical form and associated parameter values of the parametric models were fully and reliably captured by the respective non-parametric models. The PV kernels and the associated RDs quantitatively described the transformational input–output properties of the synapses and facilitated interpretation of their functional properties. In the second half of this paper, we further investigated the predictive accuracy of these non-parametric models for RIT inputs with higher MFRs and showed that this approach can be successfully applied to this case, but only if we increase sufficiently the order of the PV models to capture the higher-order dynamics and nonlinearities associated with higher input MFRs.

4.1 On Poisson–Volterra kernel model

Non-parametric method was first used to model synaptic transmission by Krausz and Friesen (Krausz and Friesen 1977). In their study, they estimated Wiener kernels of the lobster cardiac ganglion synapse using cross-correlation technique. The approach used in this study has several important differences and improvements compared to their approach. First, instead of Wiener kernels, we estimated Volterra kernels, which renders the kernel estimates invariant to input characteristics when a mathematically complete model is used. The corresponding RDs of the estimated PV kernels can be directly related to conventional electrophysiological measurements, e.g., r_1 is baseline postsynaptic response amplitude and r_2 is the paired-pulse facilitation/depression function. The utilization of RDs relaxes the requirement of mathematical completeness of the model in representation, since they remain invariant in practically complete models. By contrast, Wiener kernels highly depend on the input characteristic, e.g., MFRs of the Poisson input train. For example, first-order Wiener kernel is the mean of the response amplitudes during the Poisson train, which obviously depends on MFR. Second, in this study, the PV kernels of the non-parametric models are estimated using the Laguerre expansion technique that allows accurate and efficient kernel estimation with short datasets (Marmarelis 1993). Most of PV kernels in this paper are estimated with only 400 input–output pairs, which is a significant advantage when we consider that the conventional cross-correlation technique usually requires thousands of input–output pairs for comparable accuracy (Krausz and Friesen 1977; Berger et al. 1988a, 1988b; Sclabassi et al. 1988). In addition, the Laguerre expansion technique allows the estimation of PV models of higher orders (i.e., third and fourth order) which is extremely difficult using the conventional binning method, since the latter involves much larger number of kernel coefficients to be estimated. Compared to previously obtained second-order PV kernel models (Gholmieh et al. 2001), higher-order models provide more accurate output predictions, because they capture the higher-order nonlinearities associated with more complex input–output properties and/or higher input MFRs. This is demonstrated clearly in the SC synapse result, where there is a dramatic drop of prediction error when we increase the model order from second to third. For this specific system, only PV models of order higher than second are practically complete, in the sense that they capture the major effect of system nonlinearity. By contrast, the second-order PV model, being an incomplete model, fails to give accurate prediction. Furthermore, because of the prominent third-order nonlinearity of the SC synapse, the kernel estimates of the second-order PV model are biased by the presence of the higher-order nonlinearities. Thus, the second-order model yielded values of r_2 that are markedly different from the actual paired-pulse facilitation/depression function (Fig. 8).

It is important to point out again that the practical completeness of the PV model is also dependent on the MFR of the random inputs. When input MFR increases, the possibility of higher-order nonlinear interactions increases. In SC synapses, when the MFR of the Poisson RIT is 2Hz, the third-order PV model is practically complete, but when the MFR is increased to 10Hz, the fourth-order PV model is practically complete. This raises one important aspect of the non-parametric modeling approach: namely their guaranteed ability to predict the output is only for input patterns that are within the range of the inputs with which they are estimated. Although this is often true for parametric modeling as well, it is more critical for non-parametric modeling since non-parametric model is purely data-driven and in general lacks the extrapolation power. Therefore in experimental design, it is crucial to use broadband inputs that cover the patterns of physiological interest.

Another form of quantitative model of STP in neuromuscular junctions of a crustacean was introduced by Sen et al. (1997). This model consists of a cascade of three components: a linear filter K_2, followed by a static nonlinearity F, followed by another linear filter K_1. Filter K_1 describes the shape of the postsynaptic response, e.g., excitatory junctional current/potential (EJC/EJP), and is equivalent to the "typical EPSC waveform" that we used here to deconvolve the EPSC train in Part II of this study (see companion paper for details). The other filter K_2 is the first component of the cascade and serves to integrate the input activity over a longer past epoch. Sen et al. showed

that it has an exponential form (with a negative exponent) extending over several seconds. The output of K_2 (i.e. the integrated input past activity) is transformed by the static nonlinearity F, which was shown to exhibit a supra-linear form (exponential-like, with a positive exponent). This model form represents the linear-nonlinear (LN) cascade model studied extensively in the 70s in connection with various sensory systems (for a review, see Marmarelis and Marmarelis 1978). The PV kernels estimated in this study correspond to the cascade of K_2 and F in the sense that they describe the nonlinear dynamic transformation of a point-process input (presynaptic spike train) to varying-amplitude outputs (EPSC or EJC/EJP amplitudes) which represents the combined effect of K_2 and F. It was shown that this model can be successfully applied to several crustacean neuromuscular junctions. However, it should be noted that this LN model does not constitute a *complete* representation of arbitrary nonlinear dynamics like the Volterra modeling approach. It relies on the strong assumption that the nonlinear dynamics of a particular system can be separated into a cascade of a single linear filter followed by a single static nonlinearity. The general Volterra representation is equivalent to the Wiener–Bose model (composed of *multiple* parallel linear filters feeding into a multi-input static nonlinearity) or it can be decomposed into *multiple* parallel LN cascades termed the "principal dynamic modes" (Marmarelis 2004). We note that Sen et al. (1997) adopted the LN approach for one important and valid aim, namely, developing a methodology that is "as simple as possible both to apply and to describe" while retaining a certain degree of generality and interpretability. This aim is different from the aim of the non-parametric modeling in this study, since we seek a general and complete representation of STP that allows us to reveal the subtle features of the nonlinear dynamical characteristics and use them to guide the modification of the parametric model.

4.2 Parametric vs. non-parametric modeling

Before using experimental input–output (stimulus–response) data, in this paper, kernel models are estimated using input–output data simulated with four parametric synapse models. There are several reasons for this: first, the parametric synapse models included in this paper represent several distinct forms of STP determined by the principle physiological mechanisms/processes. They include a variety of input–output properties and make it possible to test the generality of the non-parametric approach within a broad context. Second, the parametric models are thoroughly known, stationary, nonlinear systems that allow direct and unambiguous validation of the non-parametric models. Third, the *FD* model capture the basic mechanisms of STP, i.e., residual calcium-dependent facilitation and depletion-based depression. As shown in Section 3, many insights are gained by studying the relationships between its key parameters, which represent fundamental biological processes, and the kernels, which quantitatively describe the functional input–output properties of the system.

Parametric and non-parametric approaches are developed for distinct aims and have their relative strengths and weaknesses in modeling a biological system (Berger et al. 1994), and thus can be used in a synergistic manner. In this paper, we show that the non-parametric PV model provides a quantitative description of the synaptic input–output transformation without requiring prior assumptions about the model structure. Furthermore, non-parametric model extracts the system nonlinearities and expresses them in a uniform and often simpler form. For example, the parametric *FD* model involves nonlinear differential equations; Analytical solution of output for a given input pattern is not obvious. On the other hand, using the non-parametric PV model, prediction of outputs for a given input pattern only requires simple arithmetical operations such as multiplication and summation. The uniformity and simplicity of model mathematical form is critical for large-scale simulations (Traub and Miles 1991) and hardware implementations (Tsai et al. 1998; Berger et al. 2001).

Most importantly, non-parametric models estimated directly from the input–output experimental data can be used to evaluate parametric models under broadband input conditions in terms of their input–output transformational property. The differences between the non-parametric model estimated from experimental data and the equivalent non-parametric model of the parametric model may expose unknown physiological mechanisms/processes and suggest specific modification to the parametric model. This is shown in the companion paper (part II).

Acknowledgments This research was supported by the NIH/NIBIB (BMSR), NSF ERC (BMES), DARPA (HAND), ONR, and NSF (BITS). We thank the two anonymous reviewers for their insightful comments on this manuscript.

References

Abbott, L. F., Varela, J. A., Sen, K., & Nelson, S. B. (1997). Synaptic depression and cortical gain control. *Science*, *275*, 220–224.

Barnes, C. A., Mcnaughton, B. L., Mizumori, S. J. Y., Leonard, B. W., & Lin, L.-H. (1990). Comparison of spatial and temporal characteristics of neuronal activity in sequential stages of hippocampal processing. In J. Zimmer & O. P. Ottersen (Eds.), *Understanding the brain through the hippocampal region as a model for studying structure and function* (p. 287). Amsterdam: Elsevier Science.

Berger, T. W., Baudry, M., Brinton, R. D., Liaw, J. S., Marmarelis, V. Z., Park, A. Y., et al. (2001). Brain-implantable biomimetic electronics as the next era in neural prosthetics. *Proceedings of the IEEE*, *89*, 993–1012.

Berger, T. W., Chauvet, G., & Sclabassi, R. J. (1994). A biological based model of functional properties of the hippocampus. *Neural Networks*, *7*, 1031–1064.

Berger, T. W., Eriksson, J. L., Ciarolla, D. A., & Sclabassi, R. J. (1988a). Nonlinear systems analysis of the hippocampal perforant path-dentate projection. II. Effects of random impulse train stimulation. *Journal of Neurophysiology*, *60*, 1076–1094.

Berger, T. W., Eriksson, J. L., Ciarolla, D. A., & Sclabassi, R. J. (1988b). Nonlinear systems analysis of the hippocampal perforant path-dentate projection. III. Comparison of random train and paired impulse stimulation. *Journal of Neurophysiology*, *60*, 1095–1109.

Berger, T. W., Rinaldi, P. C., Weisz, D. J., & Thompson, R. F. (1983). Single-unit analysis of different hippocampal cell types during classical conditioning of rabbit nictitating membrane response. *Journal of Neurophysiology*, *50*, 1197–1219.

Betz, W. J. (1970). Depression of transmitter release at the neuromuscular junction of the frog. *Journal of Physiology*, *206*, 629–644.

Bishop, C. M. (1995). *Neural networks for pattern recognition*. Oxford: Oxford University Press.

Creager, R., Dunwiddie, T., & Lynch, G. (1980). Paired-pulse and frequency facilitation in the CA1 region of the *in vitro* rat hippocampus. *Journal of Physiology*, *299*, 409–424.

Deadwyler, S. A., Bunn, T., & Hampson, R. E. (1996). Hippocampal ensemble activity during spatial delayed-nonmatch-to-sample performance in rats. *Journal of Neuroscience*, *16*, 354–372.

Debanne, D., Guerineau, N. C., Gahwiler, B. H., & Thompson, S. M. (1996). Paired-pulse facilitation and depression at unitary synapses in rat hippocampus: Quantal fluctuation affects subsequent release. *Journal of Physiology*, *491*(Pt 1), 163–176.

Dittman, J. S., Kreitzer, A. C., & Regehr, W. G. (2000). Interplay between facilitation, depression, and residual calcium at three presynaptic terminals. *Journal of Neuroscience*, *20*, 1374–1385.

Dittman, J. S., & Regehr, W. G. (1998). Calcium dependence and recovery kinetics of presynaptic depression at the climbing fiber to Purkinje cell synapse. *Journal of Neuroscience*, *18*, 6147–6162.

Dobrunz, L. E., Huang, E. P., & Stevens, C. F. (1997). Very short-term plasticity in hippocampal synapses. *Proceedings of the National Academy of Sciences of the United States of America*, *94*, 14843–14847.

Dobrunz, L. E., & Stevens, C. F. (1997). Heterogeneity of release probability, facilitation, and depletion at central synapses. *Neuron*, *18*, 995–1008.

Eccles, J. C., Katz, B., & Kuffler, S. W. (1941). Nature of the "endplate potential" in curarized muscle. *Journal of Neurophysiology*, *4*, 362–387.

Feng, T. (1941). The changes in the end-plate potential during and after prolonged stimulation. *Chinese Journal of Physiology*, *13*, 79–107.

Friesen, W. O. (1975). Antifacilitation and facilitation in cardiac ganglion of spiny lobster *Panulirus interruptus*. *Journal of Comparative Physiology*, *101*, 207–224.

Fuhrmann, G., Cowan, A., Segev, I., Tsodyks, M., & Stricker, C. (2004). Multiple mechanisms govern the dynamics of depression at neocortical synapses of young rats. *Journal of Physiology*, *557*, 415–438.

Gholmieh, G., Soussou, W., Courellis, S., Marmarelis, V., Berger, T., & Baudry, M. (2001). A biosensor for detecting changes in cognitive processing based on nonlinear systems analysis. *Biosensors & Bioelectronics*, *16*, 491–501.

Gover, T. D., Jiang, X. Y., & Abrams, T. W. (2002). Persistent, exocytosis-independent silencing of release sites underlies homosynaptic depression at sensory synapses in Aplysia. *Journal of Neuroscience*, *22*, 1942–1955.

Hanse, E., & Gustafsson, B. (2001). Paired-pulse plasticity at the single release site level: an experimental and computational study. *Journal of Neuroscience*, *21*, 8362–8369.

Hosoi, N., Sakaba, T., & Neher, E. (2007). Quantitative analysis of calcium-dependent vesicle recruitment and its functional role at the calyx of Held synapse. *Journal of Neuroscience*, *27*, 14286–14298.

Hsu, S. F., Augustine, G. J., & Jackson, M. B. (1996). Adaptation of Ca(2+)-triggered exocytosis in presynaptic terminals. *Neuron*, *17*, 501–512.

Hunter, J. D., & Milton, J. G. (2001). Synaptic heterogeneity and stimulus-induced modulation of depression in central synapses. *Journal of Neuroscience*, *21*, 5781–5793.

Jones, M. V., & Westbrook, G. L. (1996). The impact of receptor desensitization on fast synaptic transmission. *Trends in Neurosciences*, *19*, 96–101.

Katz, B., & Miledi, R. (1968). The role of calcium in neuromuscular facilitation. *Journal of Physiology*, *195*, 481–492.

Kirischuk, S., Clements, J. D., & Grantyn, R. (2002). Presynaptic and postsynaptic mechanisms underlie paired pulse depression at single GABAergic boutons in rat collicular cultures. *Journal of Physiology*, *543*, 99–116.

Kraushaar, U., & Jonas, P. (2000). Efficacy and stability of quantal GABA release at a hippocampal interneuron-principal neuron synapse. *Journal of Neuroscience*, *20*, 5594–5607.

Krausz, H. I., & Friesen, W. O. (1977). The analysis of nonlinear synaptic transmission. *Journal of General Physiology*, *70*, 243–265.

Lee, Y. W., & Schetzen, M. (1965). Measurement of the Wiener kernels of a nonlinear system by crosscorrelation. *International Journal of Control*, *2*, 237–254.

Liley, A. W., & North, K. A. (1953). An electrical investigation of effects of repetitive stimulation on mammalian neuromuscular junction. *Journal of Neurophysiology*, *16*, 509–527.

Lisman, J. E. (1997). Bursts as a unit of neural information: Making unreliable synapses reliable. *Trends in Neurosciences*, *20*, 38–43.

Magleby, K. L., & Zengel, J. E. (1975). A quantitative description of tetanic and post-tetanic potentiation of transmitter release at the frog neuromuscular junction. *Journal of Physiology*, *245*, 183–208.

Mallart, A., & Martin, A. R. (1967). An analysis of facilitation of transmitter release at the neuromuscular junction of the frog. *Journal of Physiology*, *193*, 679–694.

Marmarelis, V. Z (1993). Identification of nonlinear biological systems using Laguerre expansions of kernels. *Annals of Biomedical Engineering*, *21*, 573–589.

Marmarelis, V. Z. (2004). *Nonlinear dynamic modeling of physiological systems*. Hoboken: Wiley-IEEE Press.

Marmarelis, V. Z., & Marmarelis, P. Z. (1978). *Analysis of physiological systems: The white-noise approach*. New York: Plenum.

Orban, G. A., Hoffmann, K. P., & Duysens, J. (1985). Velocity selectivity in the cat visual system. I. Responses of LGN cells to moving bar stimuli: A comparison with cortical areas 17 and 18. *Journal of Neurophysiology*, *54*, 1026–1049.

Pedroarena, C. M., & Schwarz, C. (2003). Efficacy and short-term plasticity at GABAergic synapses between Purkinje and cerebellar nuclei neurons. *Journal of Neurophysiology*, *89*, 704–715.

Reid, R. C., Soodak, R. E., & Shapley, R. M. (1991). Directional selectivity and spatiotemporal structure of receptive fields of simple cells in cat striate cortex. *Journal of Neurophysiology*, *66*, 505–529.

Sclabassi, R. J., Eriksson, J. L., Port, R. L., Robinson, G. B., & Berger, T. W. (1988). Nonlinear systems analysis of the

hippocampal perforant path-dentate projection. I. Theoretical and interpretational considerations. *Journal of Neurophysiology*, *60*, 1066–1076.

Sen, K., Gibson, J., Fost, J., Abbott, L. F., Nelson, S. B., & Hunter, J. D. (1997). Synaptic heterogeneity and stimulus-induced modulation of depression in central synapses. *Journal of Neuroscience*, *17*, 7926–7940.

Song, D., Chan, R. H., Marmarelis, V. Z., Hampson, R. E., Deadwyler, S. A., & Berger, T. W. (2007). Nonlinear dynamic modeling of spike train transformations for hippocampal-cortical prostheses. *IEEE Transactions on Biomedical Engineering*, *54*, 1053–1066.

Traub, R. D., & Miles, R. (1991). *Neuronal networks of the hippocampus*. New York: Cambridge University Press.

Trussell, L. O., & Fischbach, G. D. (1989). Glutamate receptor desensitization and its role in synaptic transmission. *Neuron*, *3*, 209–218.

Trussell, L. O., Zhang, S., & Raman, I. M. (1993). Desensitization of AMPA receptors upon multiquantal neurotransmitter release. *Neuron*, *10*, 1185–1196.

Tsai, R. H., Sheu, B. J., & Berger, T. W. (1998). A VLSI neural network processor based on hippocampal model. *Analog Integrated Circuits and Signal Processing*, *15*, 201–213.

Tsodyks, M. V., & Markram, H. (1997). The neural code between neocortical pyramidal neurons depends on neurotransmitter release probability. *Proceedings of the National Academy of Sciences of the United States of America*, *94*, 719–723.

Tsodyks, M., Pawelzik, K., & Markram, H. (1998). Neural networks with dynamic synapses. *Neural Computation*, *10*, 821–835.

Varela, J. A., Sen, K., Gibson, J., Fost, J., Abbott, L. F., & Nelson, S. B. (1997). A quantitative description of short-term plasticity at excitatory synapses in layer 2/3 of rat primary visual cortex. *Journal of Neuroscience*, *17*, 7926–7940.

Volterra, V. (1959). *Theory of functionals and of integral and integro-differential equations*. New York: Dover.

Waldeck, R. F., Pereda, A., & Faber, D. S. (2000). Properties and plasticity of paired-pulse depression at a central synapse. *Journal of Neuroscience*, *20*, 5312–5320.

Wang, L. Y., & Kaczmarek, L. K. (1998). High-frequency firing helps replenish the readily releasable pool of synaptic vesicles. *Nature*, *394*, 384–388.

Watanabe, A., & Stark, L. (1975). Kernel method for nonlinear analysis: Identification of a biological control system. *Mathematical Biosciences*, *27*, 99–108.

Yamada, W. M., & Zucker, R. S. (1992). Time course of transmitter release calculated from simulations of a calcium diffusion model. *Biophysical Journal*, *61*, 671–682.

Zador, A. M., & Dobrunz, L. E. (1997). Dynamic synapses in the cortex. *Neuron*, *19*, 1–4.

Zengel, J. E., & Magleby, K. L. (1982). Augmentation and facilitation of transmitter release. A quantitative description at the frog neuromuscular junction. *Journal of General Physiology*, *80*, 583–611.

Zucker, R. S., & Regehr, W. G. (2002). Short-term synaptic plasticity. *Annual Review of Physiology*, *64*, 355–405.